Catalysis Today 139 (2008) 69–76

Contents lists available at ScienceDirect

Catalysis Today

journal homepage: www.elsevier.com/locate/cattod

Characterization and the photocatalytic activity of TiO_2 immobilized hydrophobic montmorillonite photocatalysts
Degradation of decabromodiphenyl ether (BDE 209)

Taicheng An [a,*], Jiaxin Chen [a,c], Guiying Li [a], Xuejun Ding [a,c], Guoying Sheng [a], Jiamo Fu [a], Bixian Mai [a], Kevin E. O'Shea [b]

[a] State Key Laboratory of Organic Geochemistry, Guangdong Key Laboratory of Environmental Resources Utilization and Protection, Guangzhou Institute of Geochemistry, Chinese Academy of Sciences, Guangzhou 510640, China
[b] Department of Chemistry and Biochemistry, Florida International University, Miami, FL 33199, USA
[c] Graduate School of Chinese Academy of Sciences, Beijing 100049, China

ARTICLE INFO

Article history:
Available online 20 September 2008

Keywords:
Polybrominated diphenyl ethers
Montmorillonite
TiO_2 photocatalysis
Advanced oxidation

ABSTRACT

A novel TiO_2 immobilized hydrophobic montmorillonite photocatalysts were designed and prepared for the advanced oxidation of persistent organic pollutants in water, which combined the pre-adsorption and concentrated effects for aqueous micro-organic pollutants with the photocatalytic destruction of organic pollutants. The photocatalysts were synthesized by immobilizing TiO_2 onto surfactant-pillared montmorillonite via ion exchange reaction between sodium montmorillonite with cation surfactant, cetyl trimethyl ammonium bromide (CTMAB). The Degussa P25 catalyst loading amounts varied between 20 and 80%. The composition and texture of the prepared composites were characterized with X-ray powder diffraction, scanning electron microscope, and energy-dispersive spectrometry. The adsorption performance and photocatalytic activities of prepared composite photocatalysts were evaluated using decabromodiphenyl ether (BDE 209) as a model pollutant in aqueous solution. The results were found that these composite photocatalysts can effectively degrade BDE 209, and the complete removal can be achieved within 180 min of irradiation. The removal efficiency of BDE 209 increased with the percentage of immobilized TiO_2 on the hydrophobic clay. Highly hydrophobic substrates (BDE 209) can effectively adsorb (concentrate) in or near the hydrophobic surfactant regions of TiO_2 immobilized CTMAB-pillared montmorillonite photocatalysts. The degradation pathways involving photochemical debromination and hydroxyl radical addition are proposed based on the identification of specific by-products.

1. Introduction

Polybrominated diphenyl ethers (PBDEs) are a class of persistent aromatic compounds used as flame retardants in plastics, paints, foam, textile coatings, wire and cable insulations and electrical connectors [1]. PBDEs have become widespread environmental contaminants. In 1999, the global demand for PBDEs was approximately 67,000 tons, including an estimated 54,800 tons of decabromodiphenyl ether (BDE 209) [2]. Because of their extreme lipophilicity (up to $\log K_{ow} = 9.97$ for BDE 209) [3] and limited bioavailability [4], the highly brominated congeners are generally considered to be recalcitrant but safe chemicals. Unfortunately, PBDEs migrate from products into the environment. The highly brominated congeners can be transformed to lower-brominated congeners via photochemical processes [5,6]. These lower-brominated congeners have been frequently detected in sediments, sewage sludge, fish, mammals (including humans), and air [7]. PBDEs are a serious environmental concern due to their persistence, potential for bioaccumulation [8] and possible adverse effects in humans [9]. While a number of reports have appeared describing the photochemical transformations of PBDEs [3,5,6,10], the focus of these reports is on photochemical debromination. The photolytic degradation and advanced oxidation of PBDEs has received limited attention. A fundamental understanding of the photolytic and oxidation transformations of PBDEs is critical for assessing the environmental impact (fate), associated health risks, biological transformation (metabolism) and remediation technologies of PBDEs.

Advanced oxidation processes, notably TiO_2 photocatalysis have shown tremendous promise for the remediation of persistent

* Corresponding author. Tel.: +86 20 85291501; fax: +86 20 85290706.
E-mail address: antc99@gig.ac.cn (T. An).

0920-5861/$ – see front matter © 2008 Elsevier B.V. All rights reserved.
doi:10.1016/j.cattod.2008.08.024

pollutants and represent potential solutions for the remediation of PBDEs from the environment. Semiconductor nanostructures (e.g. TiO_2) and organic-pillared montmorillonite clays have received considerable interest for the remediation of pollutants over the past several decades because of their unique properties. TiO_2 exhibits excellent photocatalytic properties for the mineralization of organic pollutants and toxins [11], while montmorillonite clays exhibit attractive absorption properties for removal of pollutants from aqueous media [10]. TiO_2 photocatalytic water treatment technologies typically involve a suspension of nanosized particles. Unfortunately such applications require removal or reclaimation of the catalyst. Montmorillonite have excellent absorption properties, but are not photoactive under typically TiO_2 photocatalytic treatment conditions. Immobilization of TiO_2 onto hydrophobic montmorillonite can prevent the release of adsorbed contaminants and enable the adsorbent to be continuously regenerated in situ [16]. In an attempt to minimize such disadvantages and maximize the cooperative photochemical and absorption properties of these materials a surfactant-modified support was synthesized. Development of TiO_2 composite photocatalysts is attractive because it can enhance adsorption properties while allowing easy separation of the photocatalyst from the treated solution [12]. Li et al. used TiO_2 dispersed onto silicate for the photodegradation of organic pollutants [13]. TiO_2 photocatalysts supported on clay can be easily recovered and reused. Because of their inert chemical nature, porous structure and well-defined surface montmorillonite layered clays, are excellent supports. The inorganic ions (sodium or calcium) between the interlayers of montmorillonite can be exchanged with alkylammonium surfactants [14], such as cetyl trimethyl ammonium bromide (CTMAB). Montmorillonite clay becomes more hydrophobic and a better absorbent for lipophilic organic pollutants after such modification [15]. As a hydrophobic support, organic-pillared montmorillonite clays enable easy immobilization of TiO_2 at the surface and interspacial regions of the clays. Such composites possess favorable absorption properties and high photocatalytic activities for degradation of organic pollutants. To exploit the advantages of TiO_2 photocatalysis and layered clays, new composites of TiO_2 immobilized onto hydrophobic montmorillonite were prepared and used for the remediation of the problematic organic pollutant, BDE 209. Here in we report detailed studies on the characterization and application of TiO_2 supported on surfactant-modified clay for the degradation of BDE 209.

2. Materials and methods

2.1. Chemicals

Raw montmorillonite, obtained from Lin'an (LA), Zhejiang, China, has the structural formula $(Na_{0.318}K_{0.034}Ca_{0.135})$ $(Al_{1.441}Fe_{0.088}Mg_{0.327})$ $Si_4O_{10}(OH)_2{\cdot}nH_2O$, surface area and cation exchange capacity (CEC) of 18.03 m^2/g and 54.47 mmol/100 g, respectively. The raw clay was ground to <200 mesh prior to use. Titanium dioxide (Degussa P25) is mainly anatase (ca. 70%) with a mean size of ca. 30 nm and a surface area of 50 m^2/g, was used as received. Decabromodiphenyl ether (98% purity) and decachlorobiphenyl (98% purity) were purchased from ACROS (Fair Lawn, NJ, USA). A standard mixture containing BDE 28, 47, 77, 99, 100, 118, 154, 187 and 209 was obtained from AccuStandard (New Heaven, CT, USA). All remaining reagents were of analytical grade and purchased from Fluka (Taufkirchen, Germany), Scharlau (Barcelona, Spain) and Aldrich (Milwaukee, WI, USA). All aqueous solutions were prepared with deionized water.

2.2. Preparation of photocatalysts

The montmorillonite clay was soaked in water (1 g/100 mL) for 24 h to induce appropriate swelling. The swelled clay was treated with excess alkylammonium salt (twice the CEC of the host clay) to promote exchange with the layered silicates in the clay. The slurry was stirred continuously for 48 h at 60 °C. The cation-exchanged clay was collected by centrifugation and subsequently washed with deionized water until bromide ions were not present in the solution. A portion of the modified clay was collected for characterization and will be referred to as the hydrophobic clay. TiO_2 was slowly added to the slurry of hydrophobic clay at TiO_2:clay weight ratios of 1:4, 2:3, 3:2 and 4:1. The slurry was stirred for another 48 h and the resulting composite separated from the suspension by centrifugation. The composite was dried in an oven at 60 °C until a constant weight was obtained. The dry composite was ground to a size less than 200 mesh, and stored in vacuum container for further use. Four composites were prepared, NLCT14, NLCT23, NLCT32, and NLCT41 with the last two numbers representing the TiO_2 to clay weight ratio. Thermal decomposition of the organic-pillared clay occurs by a series of distinct steps but requires temperatures >180 °C [17]. To ensure the stability of the composites all experiments were carried out below 180 °C.

2.3. Characterization of photocatalysts

Powder XRD patterns were obtained using a D/Max 2200 VPC powder diffractometer (Rigaku, Tokyo, Japan) with Cu Kα radiation (λ = 0.15418 nm), in the scan range 2θ between 1.5° and 15°. A Quanta-400 scanning electron microscope (FEI, Hillsboro, Oregon, USA) was used to observe the microstructure of the prepared photocatalysts operating at 20 kV. An energy-dispersive X-ray spectroscopy (EDS) was obtained using Genesis-2000 (EDAX, Mahwah, NJ, USA) which was equipped with the scanning electron microscope (SEM).

2.4. Adsorption and photocatalytic degradation experiments

Adsorption and photocatalytic degradation of BDE 209 onto the TiO_2:clay composites were conducted in a cylindrical quartz reactor (180 mL) with a double walled thermostating jacket to keep the solution temperature constant throughout all experiments. A GGZ-125 125 W high-pressure mercury lamp (Yaming Lighting Co., Shanghai, China) was housed on one side of the reactor to serve as an irradiation source. The maximum light intensity of the lamp occurs at 365 nm. Tetrahydrofuran (THF) was used as a co-solvent to enhance the solubility of BDE 209 in aqueous media. A stock solution of BDE 209 in THF was prepared at 200 mg/L [10]. A substrate solution (10 mg/L BDE 209) was prepared using the THF stock solution to obtain a deionized water:THF (95:5, v/v) solvent. The solution described above containing 0.3 g of photocatalyst was stirred and opened to the air in the dark for 60 min to achieve the air saturation and the adsorption equilibrium. Once equilibrium was established illumination was carried out and samples taken for dark control, adsorption and photocatalytic degradation experiments. Small aliquots (5 mL) were sampled for analysis.

2.5. Analytical method

The aqueous solution of composites were separated by centrifugation and analyzed independently to distinguish the contributions of adsorption and photocatalytic degradation in the removal of the substrate. The slurry was extracted with dichloromethane (3.0 mL) three times without and with centri-

fugation (separation of the photocatalysts). The extracts were dried over anhydrous sodium sulfate, filtered, and a gentle nitrogen purge used to remove the solvent. The resulting residue was taken up in 200 μL of *n*-hexane for analyses. A procedural blank and duplicate samples were processed every 20 samples to validate the analytical procedures. Decachlorobiphenyl (PCB 209) was used as an internal standard with 50 μg/L added to every sample prior to extraction. Recoveries of PCB 209 were 75.9–107.7%. Quantitative determination of BDE 209 was achieved using GC/MS with the external standard and calibration curves with a minimum of six different concentrations at low and high concentration regimes. The sample (1.0 μL) was injected into an Agilent 6890N gas chromatograph (Hewlett-Packard, Little Falls, DE, USA) equipped with a DB-XLB column (15 m × 0.25 mm, 0.10 μm) with helium as the carrier gas. An Agilent 7683B automatic split–splitless injector was used on splitless injection mode. The initial oven temperature was maintained at 180 °C for 1 min, then programmed at a rate of 20 °C/min up to 320 °C and held for another 10 min. For congener identification the oven temperature was increased at a rate of 10 °C/min up to 320 °C (10 min). An Agilent 5975 mass spectrometer (Hewlett-Packard, Little Falls, DE, USA) detector in the selected-ion monitoring (SIM) mode was employed. The mass spectrometer was operated in electron impact ionization (EI) mode with impact energy of 70 eV. Ions peaks ($[M]^+$, $[M-Br_2]^{2+}$, or $[M-Br_2]^+$) were selected. The *m*/*z* 214, 428, 498 ($[M]^+$) were observed for BDE 209 between 4 and 10 min, *m*/*z* 400($[M-Br_2]^{2+}$), 799 ($[M-Br_2]^+$) and 959($[M]^+$) for BDE 209 and *m*/*z* 79 and 81 for other possible lower-brominated congeners were present between 4 and 18 min.

The photocatalytic degradation products were also detected using API3000 LC/MS/MS system (Applied Biosystems, Foster City, CA, USA) equipped with a gradient solvent delivery system and SIL-HTA automatic injector (Shimadzu, Kyoto, Japan). The column was a Shimadzu VP-ODS C18 column (150 mm × 4.6 mm, 5 μm). The injection volume was 20 μL, and the mobile phase of acetonitrile to water (75:25) was pumped at the flow of 0.5 mL/min. The MS analysis was conducted with negative-ionization mode with electrospray interface (ESI) source. The electrospray capillary voltage was set to 4500 V. Full scanning analyses were performed by scanning *m*/*z* range from 50 to 1000 in profile mode.

3. Results and discussion

3.1. XRD analysis

XRD patterns in the small-angle range of the raw clay (LA), hydrophobic (surfactant exchanged) clay and four prepared TiO_2 immobilized hydrophobic montmorillonite composites are shown in Fig. 1. The raw and hydrophobic clays display the (0 0 1) basal reflection peak at $2\theta = 6.8^\circ$ and 2.25°, respectively, indicating the expected increase in basal spacing, from 1.3 to 3.93 nm upon the intercalation of organic cation surfactant. This expansion demonstrates that alkyl chains aggregate in the interlayer with the structure of paraffin-type bilayer [18]. Although the surfactants are successfully intercalated into the clay interlayer, the basal reflection peaks (at $2\theta = 2.25^\circ$) of prepared photocatalysts in Fig. 1 decrease gradually as the immobilized weight of TiO_2 increases. A highly ordered and oriented silicate layer structure is essential for the pillared clay to show the (0 0 1) peak [19]. As the ratio of TiO_2 to clay increases in the composites, randomly immobilized TiO_2 onto the surface of high-ordered layers forms a mixed and disordered composite, resulting in the weakening of the basal reflection peak at the XRD patterns. This decrease of basal reflection peak is also contributed to the lower percentages of the pillared clay content in the composite material as the TiO_2 increases.

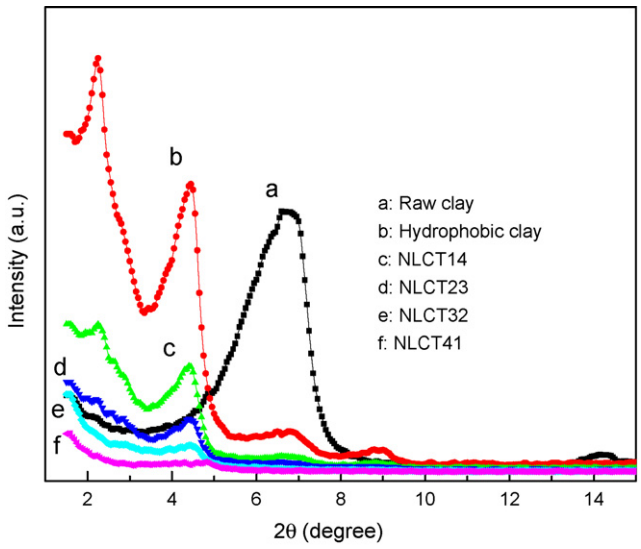

Fig. 1. XRD patterns of raw montmorillonite and prepared pillared montmorillonite photocatalysts, (a) raw clay; (b) hydrophobic clay; (c) NLCT14; (d) NLCT23; (e) NLCT32; (f) NLCT41.

3.2. SEM analysis

SEM images of raw clay (LA) and four TiO_2 immobilized hydrophobic montmorillonite photocatalysts are presented in Fig. 2. The morphologies of the composites are strongly modified by the surfactant and TiO_2, exhibiting smectite and flaky structures because of the intercalation of cation surfactant. Small aggregated TiO_2 particles are randomly dispersed on the flat plates and the interspaces of the hydrophobic organic cation-pillared montmorillonite. More particles are observed with an increase in the amount of TiO_2. Indicating the increase of immobilized TiO_2 results in less ordering of the layered clay structures, consistent with the results obtained from XRD experiments.

3.3. EDS analysis

The results of the energy-dispersive X-ray spectra for the raw clay, hydrophobic clay, NLCT14 and NLCT32 composite photocatalysts are summarized in Table 1. There are significant differences among the composition of the raw clay, the hydrophobic (surfactant exchanged) clay, and within the TiO_2 immobilized hydrophobic montmorillonite. The raw clay is composed of O (0.523 keV), Al (1.486 keV), Si (1.74 keV), Na (1.04 keV), Mg (1.254 keV) and Ca (3.69 keV) as well as minor undetectable light elements. The organic content of hydrophobic clay is estimated to

Table 1
Chemical compositions of various materials acquired from quantitative analysis of energy-dispersive X-ray spectra

Element Kα	Energy (keV)	Contents (wt%)			
		Raw clay	Hydrophobic clay	NLCT14[a]	NLCT32[a]
O	0.523	54.22	39.05	47.08	36.50
Na	1.040	1.71	ND	ND	ND
Mg	1.254	2.75	2.97	2.09	ND
Al	1.486	11.32	18.10	11.22	9.14
Si	1.740	27.95	38.14	21.85	7.17
Ca	3.690	2.04	1.74	1.04	0.84
Ti	4.510	ND[b]	ND	16.71	46.36

[a] NLCT14 and NLCT32 represent the catalyst with the last two numbers representing the ratio of TiO_2 to clay weight.
[b] Not detected.

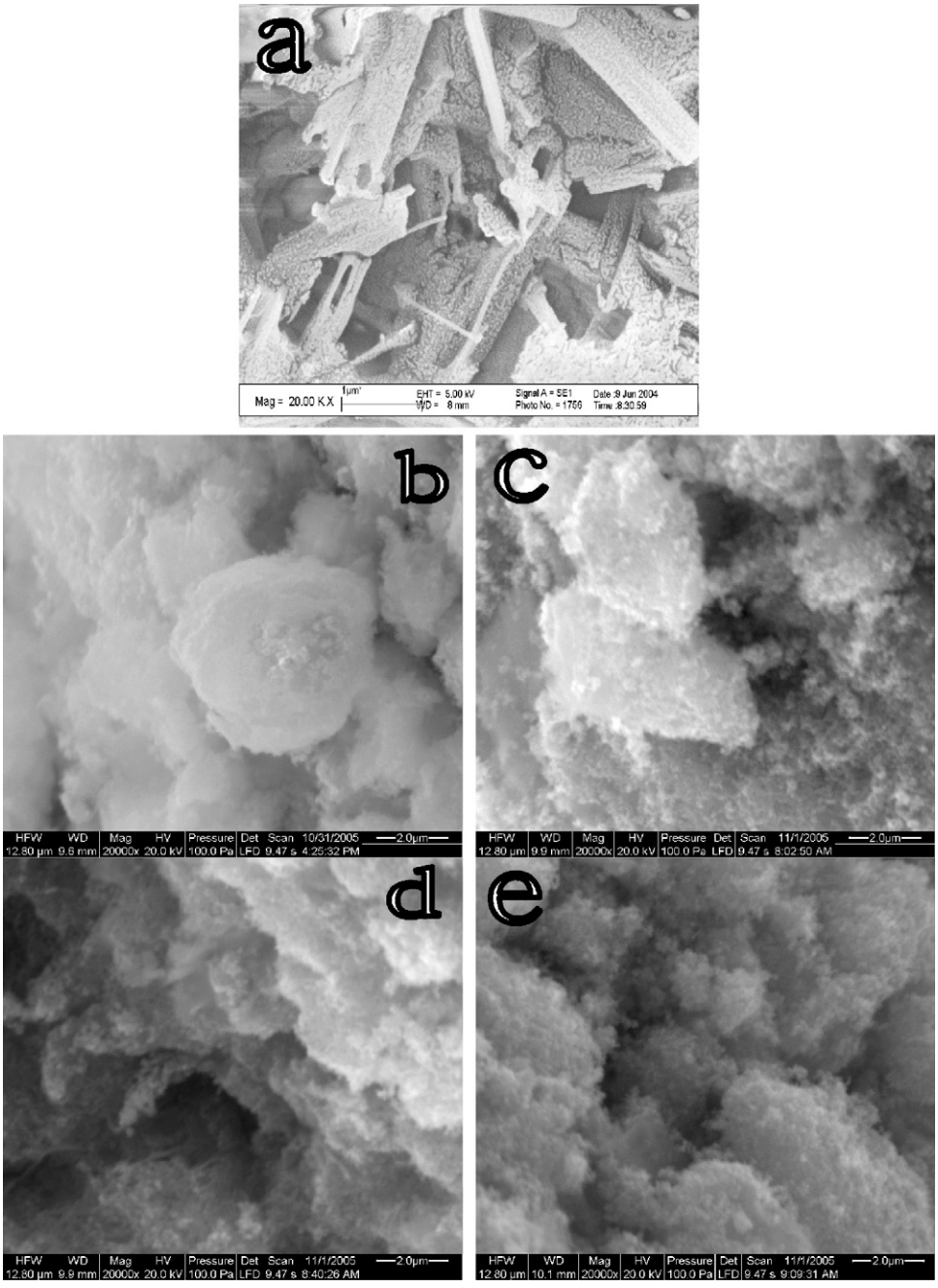

Fig. 2. SEM images of prepared photocatalysts, (a) raw clay; (b) NLCT14; (c) NLCT23; (d) NLCT32; (e) NLCT41.

be 20.73 wt% consistent with a previous study [20]. The composite photocatalysts contain primarily O, Al, Na and Ti with the presence of Ca and Na significantly reduced or absent compared to the clays. The Na is absent and a portion of the Ca (0.3%) is replaced likely exchanged/removed by the organic cation surfactant. Strong Kα signals from Ti exist at 4.51 keV, and increase with the ratio of TiO_2 present in the composite. The contents of Ti element in NLCT14 and NLCT23 are 16.7 and 46.6 wt%, respectively.

3.4. Adsorption performance of photocatalysts

The degradation of organic pollutants by TiO_2 photocatalysis occurs primarily at or near the surface of the catalyst and thus adsorption is a critical factor in the efficiency of the process [21]. The adsorption kinetic profiles of the BDE 209 onto the composite photocatalysts are presented in Fig. 3. All four composites exhibit similar adsorption behaviors for BDE 209, but slight differences in the removal efficiencies are observed. The dark adsorption rates of BDE 209 increase rapidly in the first 5 min for all the composites, and appear to reach equilibrium within 30 min. The adsorption efficiencies of all the composites are approximately 80–90%. The hydrophobic BDE 209 is expected to partition from the aqueous phase (polar) onto the composites, thus facilitating subsequent photocatalytic degradation. The nearly complete adsorption of BDE 209 may be attributed to enhanced adsorption properties of the surfactant-modified clay (smectite structure with hydrophobic character). The adsorption of BDE 209 onto the composites is governed by non-specific weak physical interactions (Van der Waals') and complementary hydrophobic properties. To evaluate the role of hydrophobic interactions in the adsorption of BDE 209,

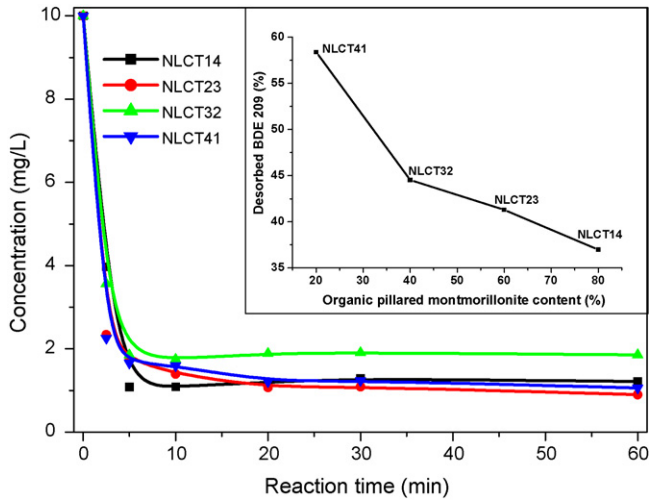

Fig. 3. The adsorption kinetics of BDE 209 onto four prepared photocatalysts.

the composites with different contents of hydrophobic clay were analyzed. The results indicate the percent of BDE 209 desorbed from composites decreases with the increase of organic montmorillonite contents (inset of Fig. 3). The adsorbed BDE 209 appears to be dependent on the hydrophobic attraction and the composites have excellent adsorption capacity for BDE 209. The affinity of BDE 209 to composites increases with the hydrophobicity of the support. That is, the higher level of organic content in the clay may be expected to adsorb more hydrophobic BDE 209. As the ratio of TiO_2 increases the adsorption decrease because less available/accessible hydrophobic sites for adsorption. Thus the strong hydrophobic interactions may prevent the release of the adsorbed contaminants to the solution again.

3.5. Degradation performance of photocatalysts

Photocatalytic performances of the TiO_2 immobilized hydrophobic montmorillonite were conducted after adsorption equilibrium and under the same conditions. The kinetic profiles for the removal of BDE 209 from the water phase by the four prepared composites are shown in Fig. 4. Approximately 38% of BDE 209 is degraded by the direct photolysis in the absence of any photocatalysts. Conduct dark controls to establish losses due to adsorption onto glassware, and found that the adsorption data obtained was below determination limits. Direct photolysis involves the UV excitation of BDE at wavelengths <300 nm and results in decomposition. Removal of BDE 209 from the water phase is completed within 180 min of irradiation for each of the TiO_2 immobilized hydrophobic montmorillonite composites. The photocatalytic degradation removal efficiencies are clearly higher than those for direct photolysis. The composite assisted removal efficiencies of BDE 209 in the solution follow this order: NLCT14 (97%) > NLCT23 (96%) > NLCT32 (85%) > NLCT41 (78%). The first two catalysts with TiO_2 to clay ratios of 20–40% preformed better than the composites with higher levels of TiO_2. The better removal performances may be related to the better adsorption capacity due to higher hydrophobic clay content in the composite with lower levels of TiO_2. On the other word, the trend also showed that the more TiO_2 were immobilized, the higher removal rates were obtained. The rate constants were 1.3, 1.9, 2.0, and 4.1 h^{-1} for NLCT14, NLCT23, NLCT32 and NLCT41, respectively.

From the above data, we can conclude that the removal of BDE 209 from solutions by the combination of adsorption and photo-initiated degradation is very efficient for all the composite photocatalysts. To evaluate the contributions of adsorption and photocatalytic degradation in the removal of BDE 209 under our experimental conditions, samples were extracted with and without centrifugal separation of composites to enable to analyze the water and mixed (particle + aqueous) phases individually. Extractions were conducted at different treatment times and the results are illustrated in Fig. 5. The role of degradation of BDE 209 becomes more important, while the adsorption becomes less important with treatment times for composites, NLCT14 and NLCT41. The degradation efficiencies for NLCT41 are higher than those with NLCT14, i.e., after 180 min ~56% of BDE 209 was degraded with NLCT41, but only 45% with NLCT14. These results are attributed to the higher level of photocatalyst TiO_2 supported in NLCT41. The contribution from degradation to the total removal of BDE 209 by NLCT41 exceeded the contribution from adsorption after 60 min of illumination with the adsorption reduced from 87 to 40%. This may be due in part to competitive adsorption by the degradation products.

Notably, the composites exhibit excellent settling properties in aqueous media and reach complete sedimentation within 24 h. The hydrophobic supports enable the immobilized photocatalysts to be easily precipitated and collected after the reaction. For

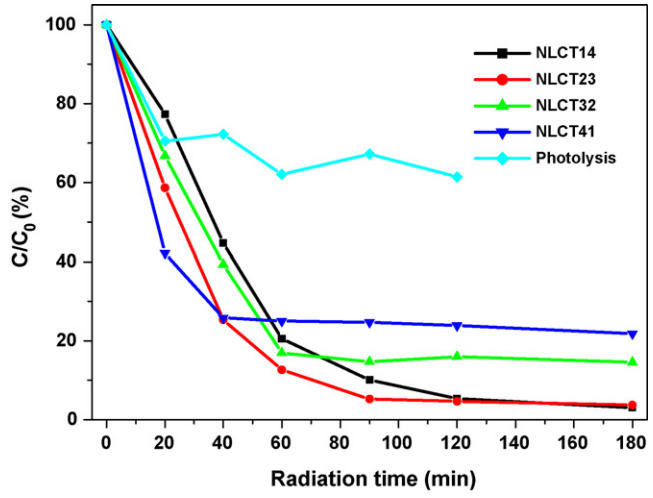

Fig. 4. The removal profiles of BDE 209 onto four prepared photocatalysts in aqueous solution.

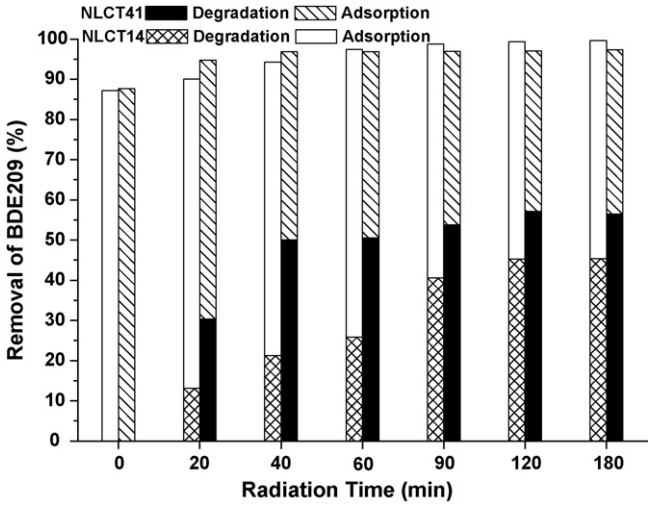

Fig. 5. Contribution from degradation and adsorption of NLCT14 and NLCT41 to total pollutant removal.

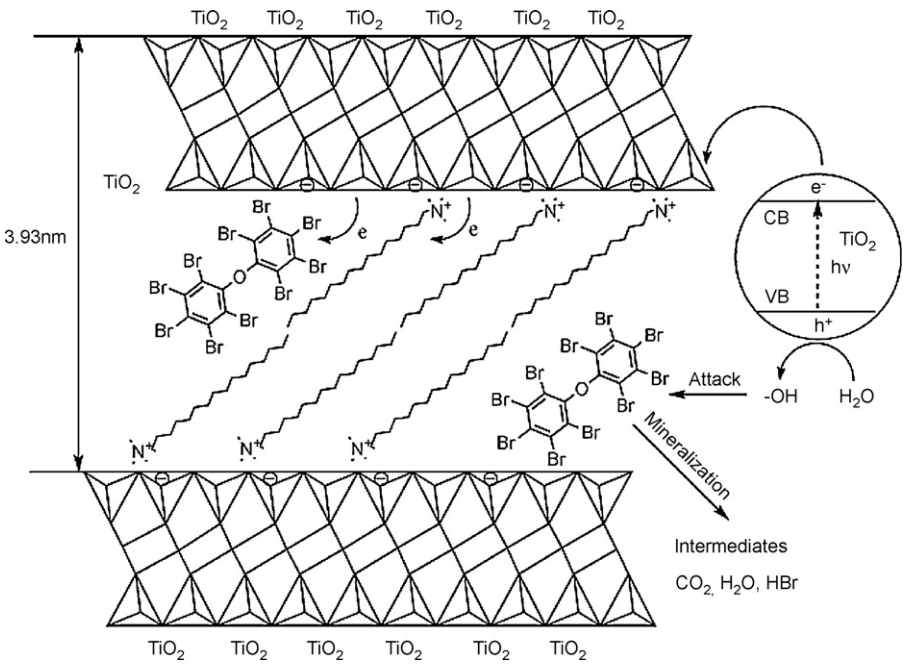

Fig. 6. Degradation scheme of BDE 209 onto organic-pillared montmorillonite supported TiO_2.

comparison aqueous solution containing raw clay and TiO_2 P25 show minimal sedimentation after 48 h.

3.6. Degradation mechanism

A number of reports have appeared on the degradation of PBDEs using different methods, including electrocatalytic hydrogenolysis [22], anaerobic degradation [23,24], reductive debromination and photochemical decomposition [25,26]. In the present system, the degradation may be facilitated by the adsorption and the transfer of organic pollutants from pillared clay interlayers to TiO_2 surfaces, as represented in Fig. 6. The hydrophobic BDE 209 tends to be strongly adsorbed onto the smectite clay, can be transferred to adjacent photocatalyst TiO_2, and undergo photocatalytic degradation. The major degradation step appears to be debromination and transformation commonly associated with reductive elimination. The montmorillonite has good electron-donating properties [27] and may mediate electron transfer during TiO_2 photocatalysis, via electron injection to BDE 209 and other organic pollutants [27,28]. The electron transfer can also occur from the electron rich clay to photoexcited BDE 209, leading to aryl–Br bond cleavage [29]. Hydroxyl radical initiated processes also appear to be important in the degradation of BDE 209 by the TiO_2 immobilized hydrophobic montmorillonite composites photcatalysts. Upon photoexcitation the TiO_2 leads to an electron–hole pair. The electron can be transferred to adjacent clay to facilitate the reductive debromination of PBDEs, while the holes are scavenged by the surface adsorbed water (hydroxyl groups) to yield $^{\bullet}OH$ radicals which can add to BDE 209 or the reaction products by addition to the aromatic ring.

3.7. Degradation intermediates and products

Prior to application of TiO_2 immobilized hydrophobic montmorillonite composites as photocatalyst for water treatment it is critical to develop a better understanding of the degradation process and reaction pathways. To investigate the reaction processes and pathways involved in the degradation of BDE 209 under our treatment conditions, GC/MS and LC/ESI/MS were used to monitor and identify the composition of the solution at different treatment times. NLCT41 was used as the model catalyst and the solution composition analyzed at different treatment times. The GC chromatograms of the samples analyzed at 120 and 180 min are compared to a standard mixture of PBDEs in Fig. 7. BDE 209 is completely removed within 120 min under our treatment conditions. While there is a significant number GC peaks in the chromatograph at 120 min of treatment that correspond to peaks in the available PBDEs standard mixture the concentrations appear to be very dilute. Most of the unidentified peaks have relative short retention times, consistent with compounds which have lower levels of bromination. After 180 min of treatment only trace peaks are observed in the GC chromatograph. Notably, BDE 28 appears to be one of the most persistent products under our experimental conditions. The qualitative interpretation of the results suggests sequential debromination is occurring in the transformation of BDE 209 and the reaction products. Such processes have been reported recently, in the transformation of deca- to hexa-brominated congeners. Our results also indicate the presence of

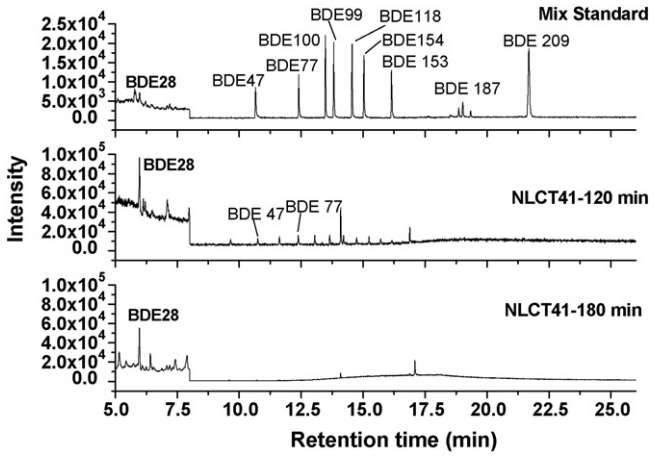

Fig. 7. GC chromatograms of standard mixture PBDE substrates, and solutions of BDE 209 after 120 and 180 min of photocatalytic treatment using NLCT41.

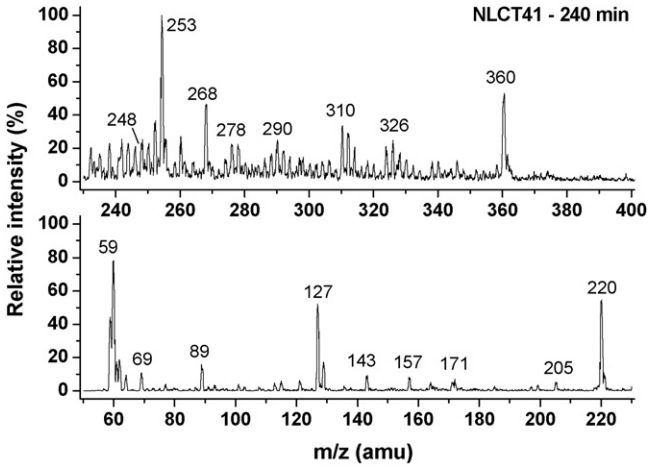

Fig. 8. ESI-MS scan spectrum of degradation intermediates (m/z from 50 to 400).

hexa-, penta-, and tetra-substituted BDE congeners, consistent with the results presented by Watanabe and Tatsukawa [30].

Major daughter intermediates produced during the further degradation were characterized on the basis of the molecular ion and mass spectrometric fragmentation pattern via ESI-MS. Typical spectra at different reaction time are illustrated in Fig. 8. While the spectra of the treated sample are too complex to be assigned completely, a number of major and important intermediates were assigned based on the comparison with authentic samples. A number of products appear to be the result of hydroxyl radical reaction products. These products include, dibromophenol ether, BBPE, m/z 360; 4,4′-dibromodiphenyl ether, BDE 15, m/z 326; bromophenoxyl benzendiol, BPB, m/z 278; bromophenoxyl phenyl, BPP, m/z 268; dibromophenol, DBP, m/z 253; 4-bromodiphenyl ether, BDE 3, m/z 248; a number of low molecular weight carboxylic acids, such as acetic acid, m/z 60; oxalic acid, m/z 90; (Z)-5-formylpent-2-enoic acid, m/z 128, etc.

3.8. Degradation pathways

Based on the identification and characterization of specific products a tentative degradation pathway of BDE 209 is described in Fig. 9. The highly brominated BDEs are transformed primarily via reductive elimination (debromination). The rates of such processes should decrease with the level of bromination because of the electronic and steric influences of the Br atoms on the aromatic system. As the level of bromination decreases the products should also become more reactive hydroxyl radical reaction pathways. In

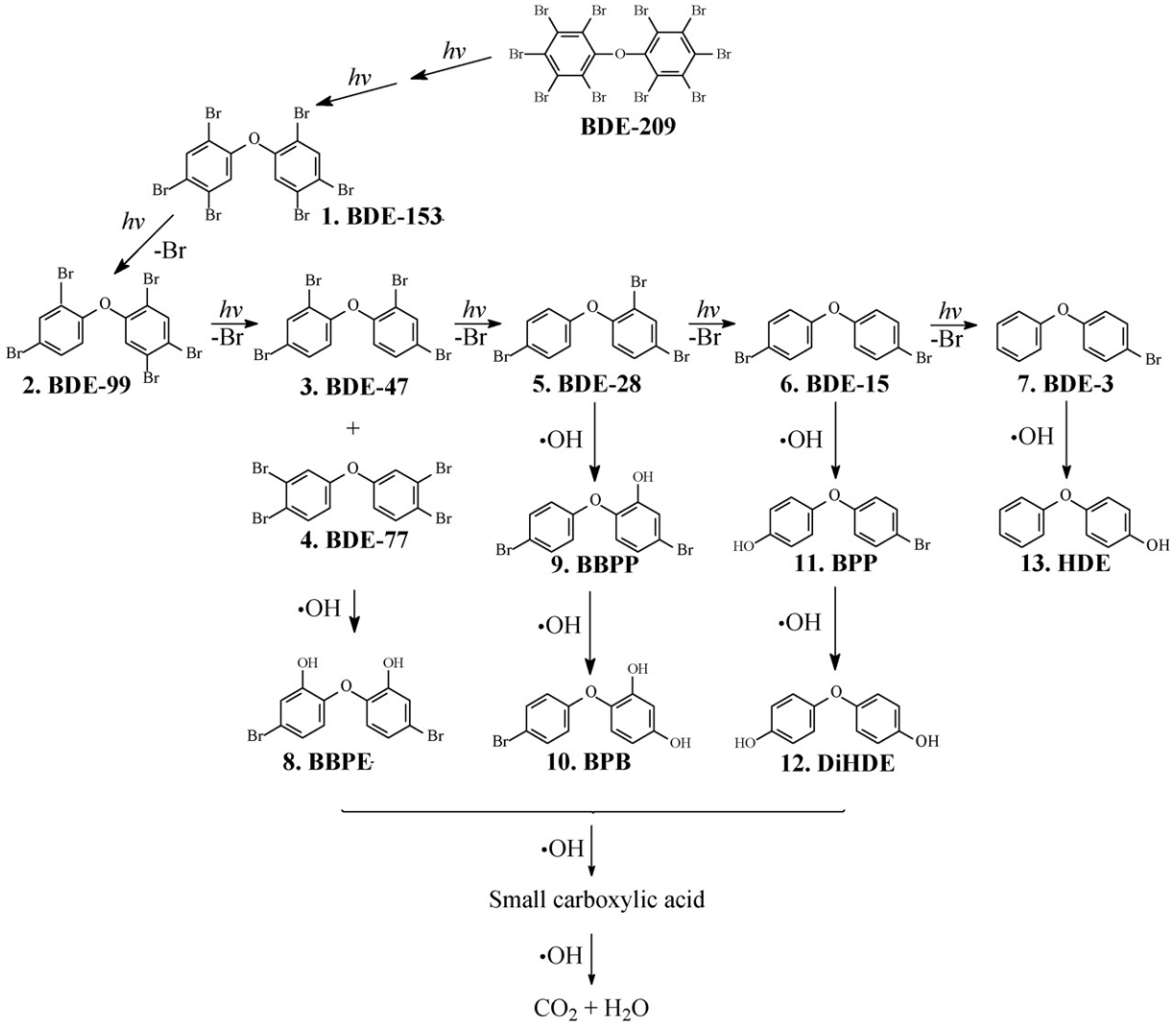

Fig. 9. Proposed mechanism for the photocatalytic degradation of BDE 209.

addition to the electronic and steric effects influencing the reaction pathways, the localization of the substrates at different regions of the composites is expected to influence the reaction pathways, i.e., for substrates localized in the hydrophobic or interspacial regions (isolated within clay layers) hydroxyl radical reactions are less likely compared to substrates localized at the external surfaces near particles of TiO_2 where hydroxyl radicals are generated. The identification of BBPE (product 8) and BPB (product 10) is clear evidence of $^{\bullet}OH$ reaction pathways. The addition of $^{\bullet}OH$ radical at the carbon ipso to Br atom of brominated aromatics has been proposed in the earlier studies [31,32]. Addition of the hydroxyl radical weakens the aryl−Br bond, which can subsequently undergo homolytic cleavage effectively replacing the bromine atom with a hydroxyl group. Such hydroxyl radical reaction pathways are consistent with a number of the products identified in the later stages of treatment, i.e., brominated phenoxy phenols (products 9 and 11) and phenoxy phenols (products 12 and 13). Further reactions of $^{\bullet}OH$ radical can induce the cleavage of aryl−O bond and lead to extensive oxidation of the aromatic ring system. The hydroxyaryloxy is a known intermediate, but the electron-donating ability of −OH group and electron-withdrawing ability of −Br group can have different effects on the bond cleavage [33]. The observed BPP is likely the result of this type reaction. Under continued treatment these products can be degraded via addition hydroxyl radical reactions ultimately leading to ring cleavage and mineralization products.

4. Conclusion

A new TiO_2 immobilized hydrophobic montmorillonite photocatalyst was successfully prepared by immobilizing TiO_2 onto CTMAB-pillared montmorillonite which was synthesized by the ion reaction with cation surfactant CTMAB. The prepared photocatalysts exhibit excellent adsorption properties for the hydrophobic contaminants, adsorbing up to 90% of our model compound BDE 209. The photocatalytic degradation efficiencies of BDE 209 were proportional to TiO_2 loading amounts immobilized onto pillared clay. The degradation mechanism was also proposed tentatively in this system. Electron transfer and hydroxyl radical reaction pathways are believed to be the major reaction processes according to the identified products in the degradation of BDE 209 under our experimental conditions.

Acknowledgments

This is contribution No. IS-091002 from GIGCAS. The authors appreciate the helpful discussions with Prof. Eddy Y. Zeng and the technology assistance from Dr. Xindong Guo, Zhifeng Du, and Mr. Tongshou Xiang. Financial support from the National Nature Science Foundation of China (Nos. 40632012, 40302013, 40572173 and 40590390) is also acknowledged.

References

[1] World Health Organization, Environmental Health Criteria 162-Brominated Diphenyl Ethers, World Health Organization, Geneva, Switzerland, 1994.
[2] M. Alaee, P. Arias, A. Sjödin, Å. Bergman, Environ. Int. 29 (2003) 683–689.
[3] I. Hua, N. Kang, C.T. Jafvert, J.R. Fábrega-Duque, Environ. Toxicol. Chem. 22 (2003) 798–804.
[4] A. Sjödin, D.G. Patterson, Å. Bergman, Environ. Int. 29 (2003) 829–839.
[5] G. Soderstrom, U. Sellstrom, C.A. De Wit, M. Tysklind, Environ. Sci. Technol. 38 (2004) 127–132.
[6] J. Bezares-Cruz, C.T. Jafvert, I. Hua, Environ. Sci. Technol. 38 (2004) 4149–4156.
[7] C.A. DeWit, Chemosphere 46 (2002) 583–624.
[8] K. Law, T. Halldorson, R. Danell, G. Stern, S. Gewurtz, M. Alaee, C. Marvin, M. Whittle, G. Tomy, Environ. Toxicol. Chem. 25 (2006) 1283–1290.
[9] P.O. Darnerud, Environ. Int. 29 (2003) 841–853.
[10] M.Y. Ahn, T.R. Filley, C.T. Jafvert, L. Nies, I. Hua, J. Bezares-Cruz, Environ. Sci. Technol. 40 (2006) 215–220.
[11] G.K. Mor, O.K. Varghese, M. Paulose, K. Shankar, C.A. Grimes, Solar Energy Mater. Solar Cells 90 (2006) 2011–2075.
[12] K. Mogyorósi, A. Farkas, I. Dékány, I. Ilisz, A. Dombi, Environ. Sci. Technol. 38 (2002) 3618–3624.
[13] J.Y. Li, C.C. Chen, J.C. Zhao, H.Y. Zhu, J. Orthman, Appl. Catal. B 37 (2002) 331–338.
[14] R.A. Vaia, R.K. Teukolsky, E.P. Giannelis, Chem. Mater. 6 (1994) 1017–1022.
[15] J.A. Smith, P.R. Jaffe, C.T. Chiou, Environ. Sci. Technol. 24 (1990) 1167–1172.
[16] C. Ooka, H. Yoshida, M. Horio, K. Suzuki, T. Hattori, Appl. Catal. B 41 (2003) 313–321.
[17] W. Xie, Z. Gao, W.P. Pan, D. Hunter, A. Singh, R.A. Vaia, Chem. Mater. 13 (2001) 2979–2990.
[18] H.P. He, R.L. Frost, T. Bostrom, P. Yuan, L. Duong, D. Yang, Y.F. Xi, J.T. Kloprogge, Appl. Clay Sci. 31 (2006) 262–271.
[19] C. Ooka, H. Yoshida, K. Suzuki, T. Hattori, Micropor. Mesopor. Mater. 67 (2004) 143–150.
[20] Q. Zhou, R.L. Frost, H.P. He, Y.F. Xi, J. Colloid Interf. Sci. 307 (2007) 50–55.
[21] C. Minero, F. Catozzo, E. Pelizzetti, Langmuir 8 (1992) 481–486.
[22] P.L.M. Bonin, P. Edwards, D. Bejan, C.C. Lo, N.J. Bunce, A.D. Konstantinov, Chemosphere 58 (2005) 961–967.
[23] A.C. Gerecke, P.C. Hartmann, N.V. Heeb, H.E. Kohler, W. Giger, P. Schmid, M. Zennegg, M. Kohler, Environ. Sci. Technol. 39 (2005) 1078–1083.
[24] S. Rayne, M.G. Ikonomou, M.D. Whale, Water Res. 37 (2003) 551–560.
[25] J. Eriksson, N. Green, G. Marsh, Å. Bergman, Environ. Sci. Technol. 38 (2004) 3119–3125.
[26] Y.S. Keum, Q.X. Li, Environ. Sci. Technol. 39 (2005) 2280–2286.
[27] N. Kakegawa, T. Kondo, M. Ogawa, Langmuir 19 (2003) 3578–3582.
[28] T. Shichi, K. Takagi, J. Photochem. Photobiol. C 1 (2000) 113–130.
[29] L. Sanchez-Prado, M. Llompart, M. Lores, C. Garcia-Hares, R. Cela, J. Chromatogr. A 1071 (2005) 85–92.
[30] I. Watanabe, R. Tatsukawa, Bull. Environ. Contam. Toxicol. 39 (1987) 953–959.
[31] J.D. Raff, R.A. Hites, J. Phys. Chem. A 110 (2006) 10783–10792.
[32] J. Peller, O. West, P.V. Kamat, J. Phys. Chem. A 108 (2004) 10925–10933.
[33] N. Haga, H. Takayanagi, J. Org. Chem. 61 (1996) 735–745.